Nanoscale

www.rsc.org/nanoscale

Volume 4 | Number 21 | 7 November 2012 | Pages 6667–6888

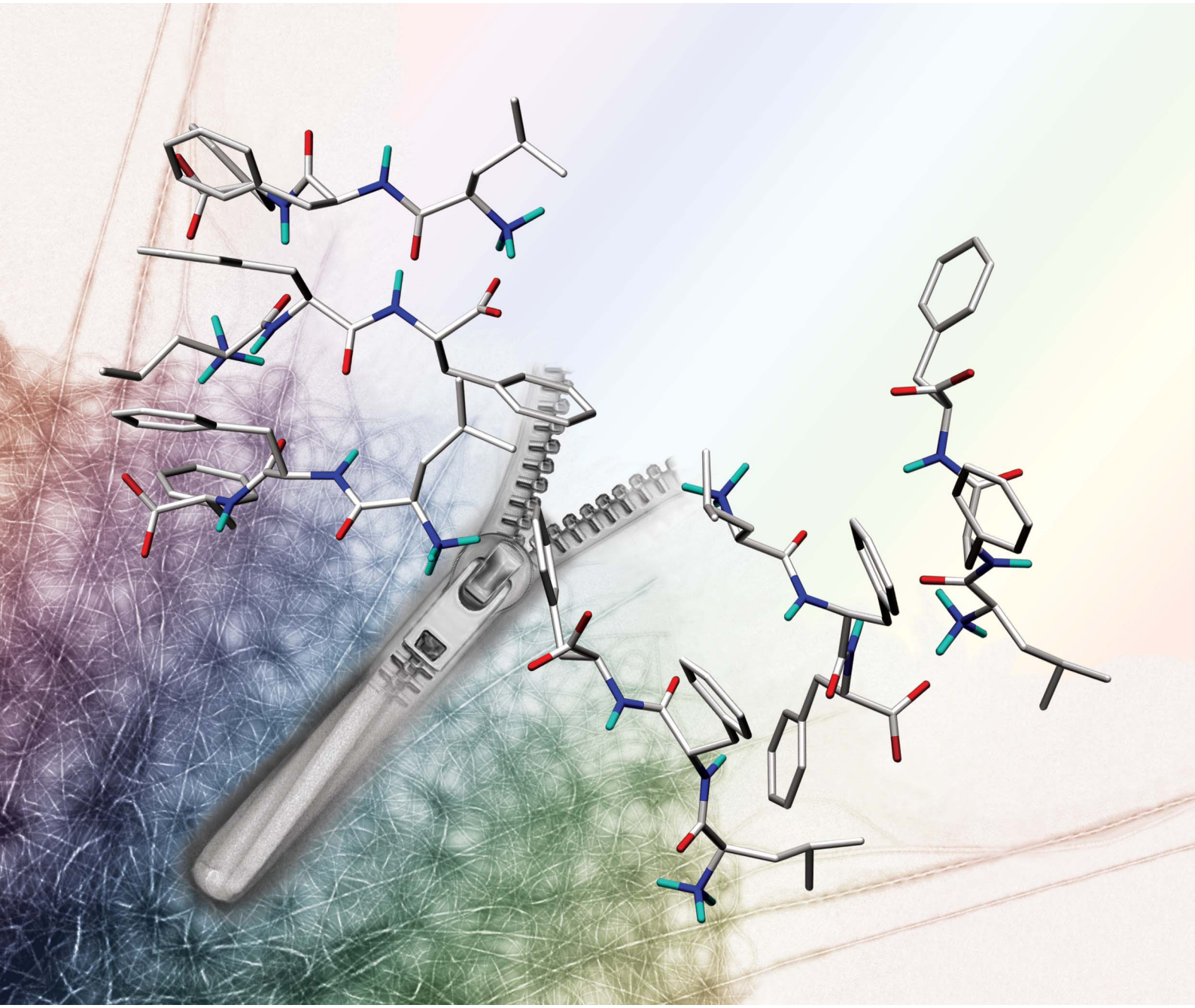

ISSN 2040-3364

COVER ARTICLE

Marchesan *et al.*

Unzipping the role of chirality in nanoscale self-assembly of tripeptide hydrogels

RSC Publishing

NCNST

2040-3364(2012)4:21;1-H

Nanoscale

Dynamic Article Links

Cite this: *Nanoscale*, 2012, **4**, 6752

www.rsc.org/nanoscale

PAPER

Unzipping the role of chirality in nanoscale self-assembly of tripeptide hydrogels†

Silvia Marchesan,*[a] Lynne Waddington,[a] Christopher D. Easton,[a] David A. Winkler,[ab] Liz Goodall,[a] John Forsythe[c] and Patrick G. Hartley[a]

Received 25th July 2012, Accepted 10th August 2012
DOI: 10.1039/c2nr32006a

Change of chirality is a useful tool to manipulate the aqueous self-assembly behaviour of uncapped, hydrophobic tripeptides. In contrast with other short peptides, these tripeptides form hydrogels at a physiological pH without the aid of organic solvents or end-capping groups (*e.g.* Fmoc). The novel hydrogel forming peptide ^{D}Leu-Phe-Phe (^{D}LFF) and its epimer Leu-Phe-Phe (LFF) exemplify dramatic supramolecular effects induced by subtle changes to stereochemistry. Only the D-amino acid-containing peptide instantly forms a hydrogel in aqueous solution following a pH switch, generating long fibres (>100 μm) that entangle into a 3D network. However, unexpected nanostructures are observed for both peptides and they are particularly heterogeneous for LFF. Structural analyses using CD, FT-IR and fluorescent amyloid staining reveal anti-parallel beta-sheets for both peptides. XRD analysis also identifies key distances consistent with beta-sheet formation in both peptides, but suggests additional high molecular order and extended molecular length for ^{D}LFF only. Molecular modelling of the two peptides highlights the key interactions responsible for self-assembly; in particular, rapid self-assembly of ^{D}LFF is promoted by a phenylalanine zipper, which is not possible because of steric factors for LFF. In conclusion, this study elucidates for the first time the molecular basis for how chirality can dramatically influence supramolecular organisation in very short peptide sequences.

Introduction

Peptide self-assembled hydrogels are a promising class of soft biomaterials for cell culture, regenerative medicine, or drug delivery applications.[1–4] In particular, peptides or peptidomimetics as short as two or three amino acids are useful in forming hydrogels due to the low cost and simplicity of preparation.[5–7] Moreover, it has been recently suggested that tripeptides have a privileged role in biology as minimal signals exploited by nature.[8] For these reasons they can be convenient building blocks in biomaterial applications. Typically, hydrophobic short peptides containing aromatic groups undergo π–π interactions that favour stacking. Many very short gel-forming peptides utilise synthetic end-capping groups (*e.g.* Fmoc, naphthalene, *etc.*) to increase molecular hydrophobicity and/or to promote this π–π stacking.[9–13] However, the potential *in vivo* toxicity of the capping groups in biomaterial applications has been suggested by reduced cell viability observed in cultures on these gels.[14,15] Alternatively, traces of organic solvents are required to assist peptide dissolution and/or supramolecular ordering.[6,14,16] There is one recent report of nanofibers composed of phenylalanine as a single amino acid, but no hydrogel is formed by this system.[17]

At the supramolecular level, the general consensus is that very short gel-forming peptides aggregate into anti-parallel beta-sheets where the peptide backbone is orthogonal to the fibril axis, in the so-called "cross-beta" structure. Hierarchical assembly of these structures results in fibrils that often display helical ordering due to the preferred right-handed twist of beta-sheets.[18] These fibrils further align into bundles and/or entangle in a 3D network, giving rise to a macroscopic hydrogel.[19]

However, subtle differences in the peptide sequence or self-assembly conditions can lead to very different supramolecular ordering, in which the role of aromatic interactions is complex.[20,21] For example, nanotubes, ribbons and even nanospheres have been reported for the dipeptides Phe-Phe, Fmoc-Phe-Phe and Boc-Phe-Phe respectively.[19,22,23] It is, therefore, not surprising that different molecular models have been proposed to account for the variety of nanostructures observed, and each self-assembly system needs to be evaluated independently.[19,24,25]

[a]*CSIRO Materials Science and Engineering, Bayview Avenue, Clayton, VIC 3168, Australia. E-mail: Silvia.Marchesan@csiro.au; marchesan.silvia@gmail.com*
[b]*Monash Institute of Pharmaceutical Sciences, 384 Royal Pde, Parkville, VIC 3052, Australia*
[c]*Monash University, Department of Materials Engineering, PO Box 69M, VIC 3800, Australia*

† Electronic supplementary information (ESI) available: video showing instant gelation for ^{D}LFF (and not LFF), following a pH trigger. Spectroscopic analysis of the two tripeptides. Microscopy images. *d* spacings from XRD diffraction analysis. Distances obtained for the energetically minimised molecular models. See DOI: 10.1039/c2nr32006a

We recently reported the first system of peptides as short as three amino acids, capable of self-assembly into a hydrogel under physiological conditions without the aid of organic solvents or capping groups.[26] These tripeptides (^{D}Val-Phe-Phe, ^{D}VFF and ^{D}Phe-Phe-Val, ^{D}FFV) form hydrogels following a pH trigger, whilst their natural L-amino acid counterparts VFF and FFV fail to do so under the same conditions. This is also the first report to show that a change of chirality in a single amino acid can drive a remarkable difference in supramolecular behaviour. However, as no nanostructure could be identified for the L-analogues, the physicochemical basis for the effect of amino acid chirality on the supramolecular organisation of these systems was still unclear.

We now report that the same strategy of changing the *N*-terminal amino acid chirality from L to D to drive self-assembly can also be applied to LFF. pH triggering results in a hydrogel at pH 7.4 for ^{D}LFF only (see video†). In this case, the effect is very dramatic as gelation occurs instantly after the pH trigger, and results in clear and enduring fibrils. Importantly, we find that LFF is, in fact, also capable of limited self-assembly, but that the resulting supramolecular order is not persistent and stable enough to yield a macroscopic gel. Moreover, microscopic monitoring of the self-assembly behaviour over time reveals the highly heterogeneous nature of LFF (as previously proposed for the non-gelling peptide VFF). We have also used spectroscopic and XRD analyses, together with molecular modelling, to identify the key intermolecular interactions that are responsible for the different supramolecular behaviours of these systems. In particular, we propose that a phenylalanine zipper may be an important interaction motif responsible for formation of robust elongated fibers in the D-epimer. We believe that this report will significantly diversify the rational design criteria which can be employed to produce novel peptide hydrogels for biomaterial applications.

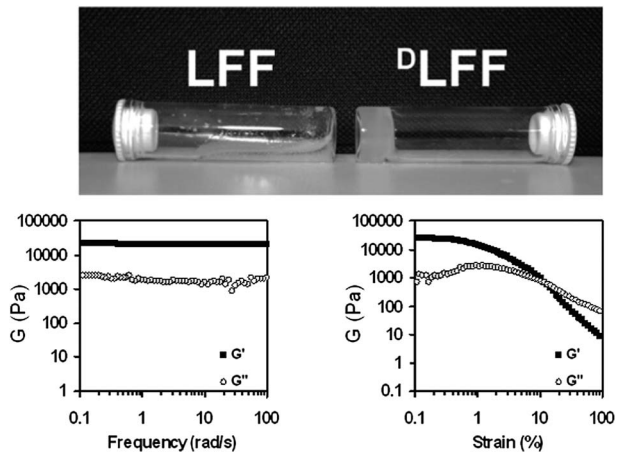

Fig. 1 Following a pH trigger, only peptide ^{D}LFF (15.7 mM) forms a self-supporting hydrogel (top), as confirmed by rheological analysis after 24 h (bottom).

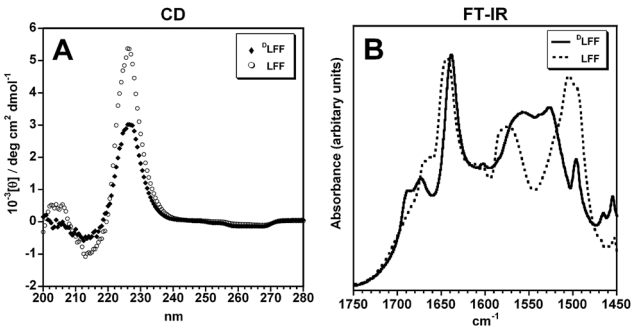

Fig. 2 (A) CD and (B) FT-IR spectra of the two tripeptides.

Results and discussion

Following the pH switch from alkaline (~12) to a final pH of 7.4, ^{D}LFF instantly forms a self-supporting translucent hydrogel (Fig. 1, top, and video†) with an elastic modulus of over 10 kPa, which increases up to 20 kPa over 24 h (Fig. 1, bottom). In contrast, LFF does not show any sign of gelation, and it behaves as a non-viscous liquid that forms a white precipitate over time.

Despite the striking difference in macroscopic behaviour, CD analysis of the two samples yields surprisingly similar spectra (Fig. 2A). Both peptides display a minimum in the region of 210–220 nm representative of beta-sheets (consistent with what was observed previously for the gelling peptides ^{D}VFF and ^{D}FFV).[26] The peak at 226 nm indicating π–π stacking of the Phe residues is also present in both samples. Overall, LFF generates a markedly more intense signal than that of ^{D}LFF, due to light scattering of the translucent hydrogel.

FT-IR analysis of the amide I region (Fig. 2B) confirms the presence of anti-parallel beta-sheets in both samples (1637 cm^{-1} and 1690 cm^{-1}), while only the non-gelling peptide LFF also displays a signal of comparable intensity at 1641 cm^{-1} for random coils. The N–H amide II region of the gelling peptide ^{D}LFF is dominated by a broad central signal (1527 and 1558 cm^{-1}), similar to that previously observed for the gelling peptides ^{D}VFF and ^{D}FFV, and compatible with the beta structure.[27] In contrast, the non-gelling peptide LFF has two distinct peaks further apart, centered at 1505 cm^{-1} and at 1577 cm^{-1}, the latter being ascribed in self-assembling short peptides to COO^{-}/NH_3^{+} head-to-tail interactions, which cause a downshift of the asymmetric stretching of the COO^{-}.[28] As terminal salt bridges are very likely to occur in ^{D}LFF too, it is possible that the same signal is further shifted to 1558 cm^{-1} for the gelling peptide, indicative of a greater extent of supramolecular interactions for this peptide, in agreement with XRD data and molecular modelling, as discussed further below.[26,28]

The amyloid stain Thioflavin T is employed to assess the extent of beta-sheet formation, since it fluoresces when bound to at least four consecutive beta-strands.[29] Confocal microscopy reveals that both peptides give rise to fluorescent structures, albeit of very different nature, and which are confirmed by AFM and TEM.

As ^{D}LFF gels immediately, microscopic bundles of fibers with thicknesses up to 2 μm and various lengths up to ~150 μm (Fig. 3A–C) can be observed by Thioflavin T fluorescence in fresh samples and samples kept for up to 7 days. Thorough analysis of fresh samples reveals nucleating regions where clusters of globular structures of varying diameter up to 3 microns can be observed (see arrows and the inset in Fig. 3B), confirmed by AFM analysis (Fig. 3D–F). It appears that fibers originate from the globules (Fig. 3D and E), suggesting that the latter occur during the very initial stages of self-assembly, in a similar

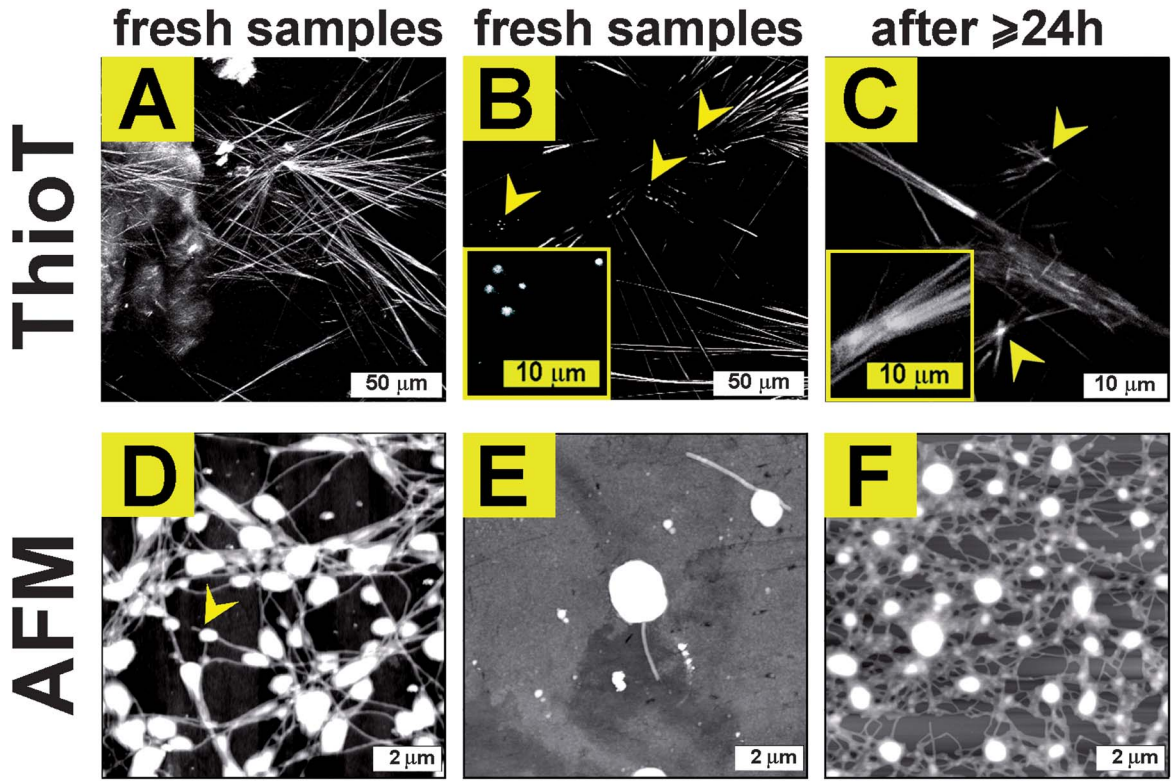

Fig. 3 Microscopy analysis (Thioflavin T fluorescence, ThioT, top, and AFM, bottom) of fresh samples of ^{D}LFF reveals a dense network of >100 μm long, enduring fibrils that appear to originate from persistent globular structures (yellow arrows and boxes). AFM *Z*-scale range is 20 nm for (D) and (E), and 60 nm for (F) (due to increased density and thickness of the observed structures).

fashion as to what was previously observed for amyloid beta (1–40) and also for a short peptide.[30,31] After 24 h, the fibrillar network density notably increases, as shown by the higher elastic modulus. Surprisingly, the globular structures are persistent, and can be seen embedded in the fibrillar network at later time points (*i.e.* over days, Fig. 3C), occurring especially at the focal points of fiber junctions (Fig. 3F).

Cryo-transmission electron microscopy and negative stain TEM (Fig. 4 and ESI, page S6†) confirm the features mentioned above at a nanoscale level. Importantly, the globular structures display electron radiation damage expected for peptides (see ESI, page S6†), and not hexagonal ice contamination, which superficially may resemble these structures. Over time, individual fibers can intertwine (blue arrows and Fig. 4C). As fiber bundles grow thicker, only a few arise from parallel fibers, while the majority display a helical period that is persistent within the same bundle, but not across separate units (Fig. 4F).

In contrast, samples of the non-gelling peptide LFF display the presence of only a few, isolated and heterogeneous nanostructures, as seen by Thioflavin T fluorescence (Fig. 5, top), AFM (Fig. 5, bottom) and TEM (Fig. 6). Fresh, stained LFF samples generally lack fluorescence, except for occasional well defined, clustered, globular structures similar to those described above (Fig. 5A and ESI, page S7†). Occasionally, crystalline needles can also be observed in fresh samples (Fig. 5B). Importantly, LFF does not develop the persistent network of elongated fibrils found for ^{D}LFF. Instead, very occasional undefined fluorescent structures arise in fresh samples near nucleating regions (inset in Fig. 5B), suggesting that very thin, transient protofibrils may be formed. This is confirmed by AFM (Fig. 5D and E) and TEM (Fig. 6). Globular structures persist over several days but can be found only as isolated, albeit more numerous, clusters (Fig. 5C, inset, 5F and ESI, page S6†). Interestingly, these structures often occur near crystal plates that arise from the alignment of the needles (Fig. 5C and ESI, page S7†). Importantly, all these structures display fluorescence when bound to Thioflavin T, indicating an extended beta-sheet nature, confirming the results of CD and FT-IR analyses.

Cryo-TEM is also in agreement with these observations (Fig. 6A–C). Nanostructures were rarely observed in fresh samples, but arise over the course of days. Interesting structural details are unveiled by negative staining (Fig. 6D–F, and ESI, page S8†). In general, heterogeneous aggregates similar to those described above are seen, including globules (A and D, and ESI, page S8†), and crystalline needles (B and E) that tend to align into plates (C and F). Thorough cryo-TEM analysis of LFF occasionally reveals, in addition, unresolved structures (Fig. 6B, inset), which resemble on a smaller scale, what is observed by Thioflavin T fluorescence microscopy (Fig. 5B, inset); negative staining revealed that these structures are compatible with thin protofilaments originating from the globules (insets in Fig. 6D and E, and ESI, page S8†). Isolated fibers are rarely seen (data not shown). However, it is important to note that samples of the non-gelling peptide LFF display self-assembly only in a few isolated regions, suggesting that these cohesive states are not the predominant forms adopted by this peptide.

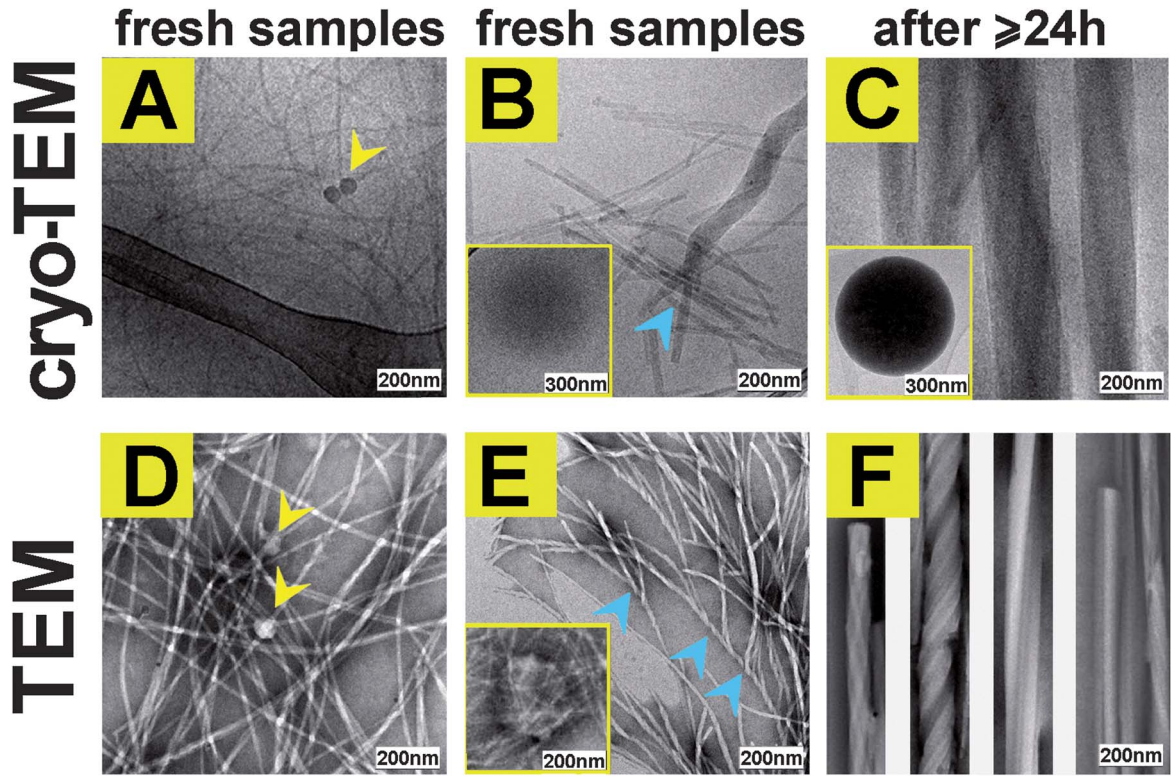

Fig. 4 Cryo-TEM analysis (A–C, top) and negative stain TEM analysis (D–F, bottom) on ^{D}LFF samples confirm the structural features observed by Thioflavin T fluorescence and AFM, namely globules (yellow arrows and insets) from which long, persistent fibers originate. Individual fibers (A and D) also intertwine (blue arrows in B and E) into thicker bundles (C and F).

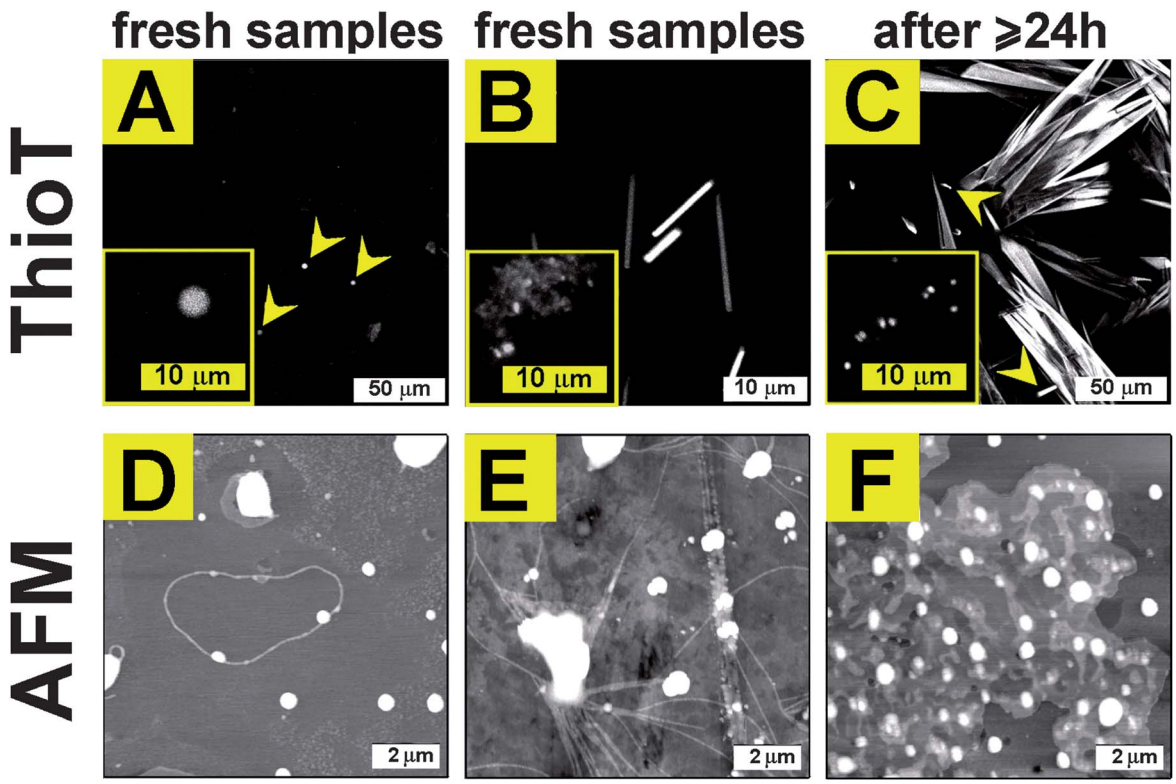

Fig. 5 Microscopy analysis (Thioflavin T fluorescence, ThioT, top, and AFM, bottom) of fresh samples of LFF reveals heterogeneous structures, including globules (yellow boxes, and A, D–F), and crystal needles (B) that tend to align into plates (C). Transient protofibrils can occasionally be seen (D and E). AFM *Z*-scale range is 20 nm for D–F.

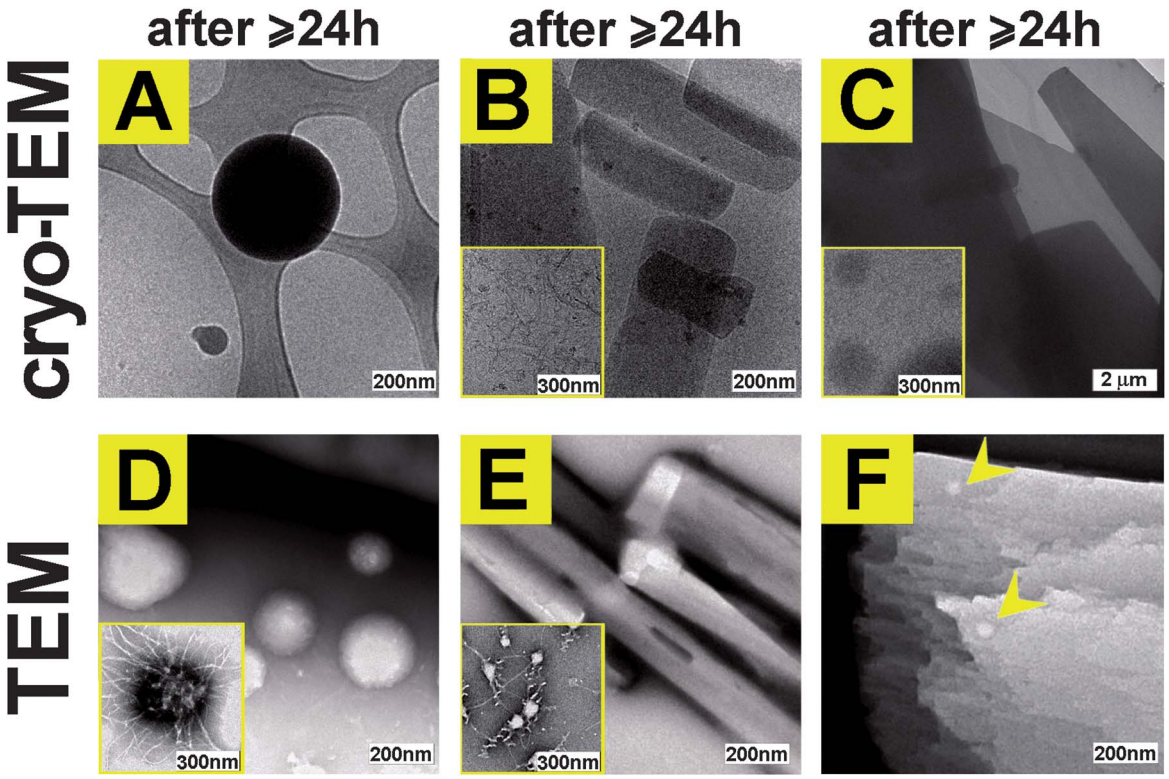

Fig. 6 Cryo-TEM images (A–C, top) and negative stain TEM images (D–F, bottom) on LFF samples reveal their heterogeneous nature: globules (A and D) with emerging transient protofibrils (insets in B, D and E), crystal needles (B and E), and crystal plates (C and F) can be seen. At later time points, more numerous clusters of globules occur in proximity of the plates (inset in C, yellow arrows in F).

Finally, XRD analysis confirmed the amyloid nature of both tripeptides (Fig. 7 and ESI†). Typical reflections corresponding to the hydrogen bonding distance between beta-strands are seen (4.9 Å and 4.6 Å for ^{D}LFF and LFF respectively). Anti-parallel arrangement is suggested by the presence of reflection at 9.8 Å for ^{D}LFF and at 9.5 Å for LFF; this signal is generally observed only in highly ordered supramolecular assemblies, and it is unusually intense for ^{D}LFF.[32] The peak at 3.8–3.9 Å is present for both peptides, and it has been correlated to the distance between planar π-stacked Fmoc groups in self-assembling dipeptides, thus it likely corresponds to the π-stacked aromatic rings of phenylalanine residues.[20] LFF also shows a prominent peak at 16.7 Å with 4 reflections, compatible with the length of the repeating unit along the peptide backbone; however, the overall weakness of the LFF diffraction signal suggests a lower order for this peptide, as also suggested by microscopic analysis. Interestingly, ^{D}LFF displays a prominent peak at 19.5 Å with up to 8 intense reflections, indicative of a high supramolecular order and of the stacking of multiple fibers along the long axis, as observed by TEM. We propose that ^{D}LFF has a more extended 3D structure (with a molecular length of 19.5 Å), as the peptide side chains can interact favourably within each other across different sheets, thus giving rise to the formation of extended fibrils as soon as self-assembly is triggered.

Molecular modelling of the two tripeptides clearly illustrates this point (Fig. 8 and ESI†). In both cases, a secondary structure of anti-parallel beta-sheets (as shown by CD, FT-IR,

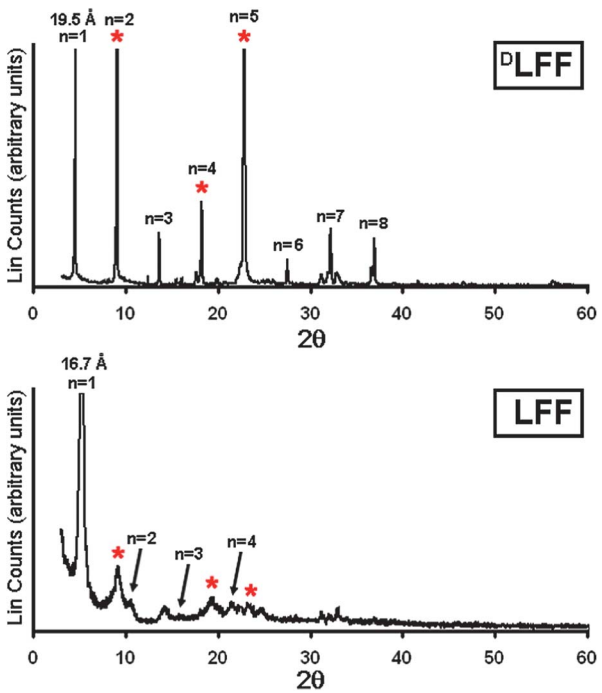

Fig. 7 XRD analysis of dried gels showing amyloid characteristic signals (*) at 9.8, 4.9, 3.9 Å for ^{D}LFF (top) and 9.5, 4.6, 3.8 Å for LFF (bottom).

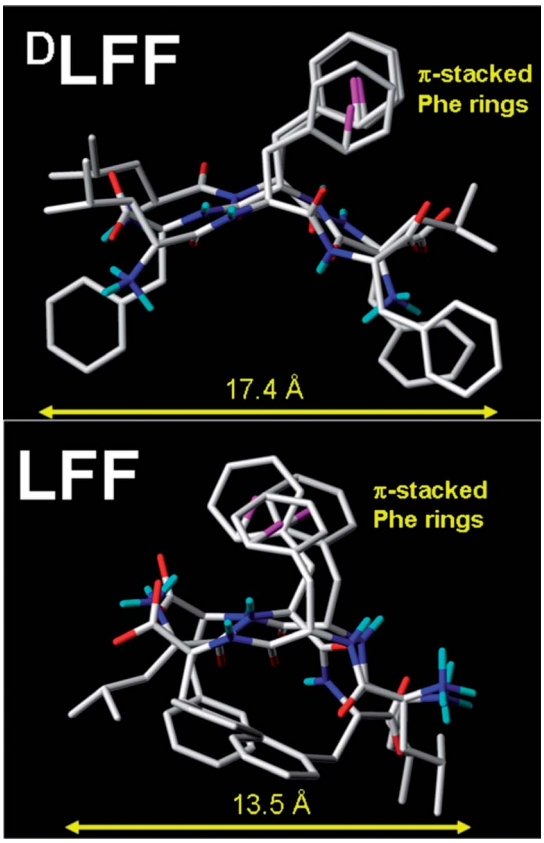

Fig. 8 Energy minimized molecular models for three anti-parallel beta-strands of ^{D}LFF (top) and LFF (bottom).

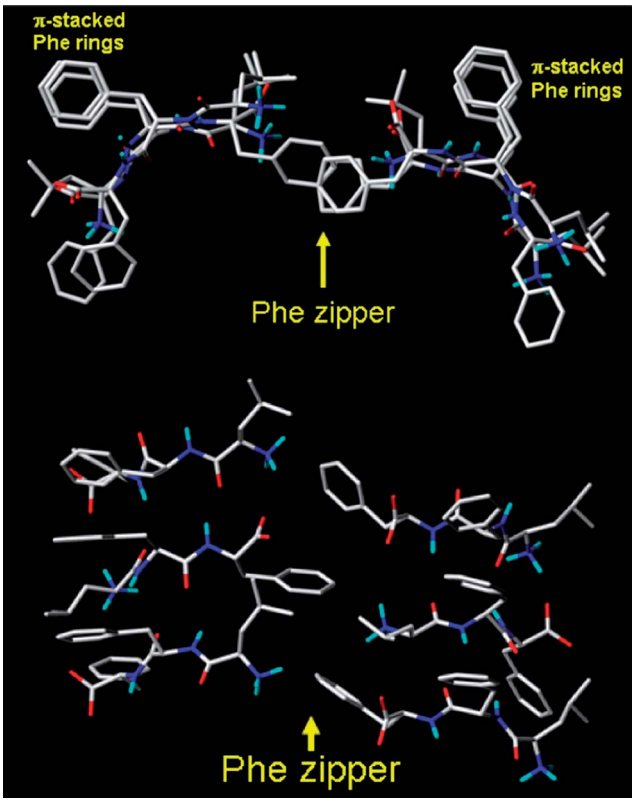

Fig. 9 Side view (top) and top view (bottom) of the energy minimized molecular model of ^{D}LFF showing a phenylalanine zipper between two anti-parallel beta-sheets.

and Thioflavin T fluorescence) would allow for π–π stacking of the central phenylalanine rings, for the formation of terminal salt bridges, and for extended hydrogen bonding between amide groups. Energy minimisation suggests a more extended molecular length and longer inter-strand distances for ^{D}LFF, in agreement with XRD analysis. Moreover, the supramolecular organisation of LFF appears somehow more disordered, thus more likely prone to a transient nature, as suggested by our experimental data. Interestingly, the extended conformation of ^{D}LFF would expose the terminal phenylalanine rings, creating a pocket in between them, where the terminal phenylalanine ring of another sheet could interlock in a knob-into-hole fashion (Fig. 9).[33] This would not be possible for its epimer LFF, due to steric hindrance from the side chain of the L-leucine.

Phenylalanine zippers, named after the well-known leucine zippers, are key elements that ensure cohesion of secondary structures by interlocking the aromatic side chains of adjacent peptide backbones. Typically, they hold together alpha-helices or coiled-coils.[34–37] We have located only one report where a phenylalanine zipper is proposed to occur between anti-parallel beta-sheets, and that applies to an amyloid peptide containing the FF motif.[38] The more generic term of "steric zipper" has been used to describe interdigitated amyloid beta-sheets in several peptides related to degenerative diseases, although no cases of this kind are known for sequences as short as three amino acids.[39]

Conclusions

In conclusion, we have elucidated the role of chirality in triggering self-assembly of hydrophobic tripeptides containing a D-amino acid at their *N*-terminus using the gelling peptide ^{D}LFF, and its analogue LFF. We show that, following rapid pH lowering to 7.4, only the former gives rise to a self-supported hydrogel, similar to what was previously reported for ^{D}VFF and ^{D}FFV.[26] However, in our study hydrogelation occurs instantly after the pH trigger, and nanostructures are identified for both peptides. Their transformations over time were also monitored by microscopy. Not only does our study identify chirality as a key element in self-assembly and modulation of nano-morphology, but it also provides insights into the initial stages of self-assembly. Both LFF and ^{D}LFF appear capable of extended beta-sheet formation, as confirmed by Thioflavin T binding and fluorescence, FT-IR, and CD analyses. During the initial stages of self-assembly, both peptides form globular structures, however only ^{D}LFF progresses towards fibrillisation and macroscopic gel formation. AFM, cryo-TEM and TEM with negative staining, all confirm this behaviour and reveal only occasional, short, thin filaments from the L-analogue. Indeed, LFF filaments do not have the ability to persist over time, and to extend over space, to the extent required to cause gelation. It is tempting to speculate that the overall morphological transition pathways of these two tripeptides are similar to those in longer amyloids.[40,41] In particular, we suggest that LFF may self-assemble *via* different kinetic pathways. Initially, nucleating

regions are formed where phase separation of peptide molecules into globules occurs. Next, these globular structures evolve into clusters, or nucleate short, thin filaments. However, over time peptide aggregates rearrange into needle-like crystals that align into plates where this is the most thermodynamically favoured supramolecular peptide ordering. Likewise, ^{D}LFF displays formation of peptide globules during the initial stages of self-assembly. However, we propose that this peptide presents a more extended 3D molecular structure (as supported by XRD analysis and molecular models). This allows the peptide molecules to quickly rearrange, and interlock more effectively into elongated fibers, resulting in a robust structure over space and time. Importantly, we identify a phenylalanine zipper as an important interaction motif between interdigitated beta-sheets of the peptide for ^{D}LFF, but not its sterically hindered L-epimer. Where this interaction is possible, it promotes immediate macroscopic gelation and the system slowly evolves as to have a higher fiber density and larger fiber bundles.

This study confirms the key role of chirality as a crucial tool to drive self-assembly of short hydrophobic peptides into aqueous hydrogels of physiological pH. Furthermore, we envisage that this work will help elucidate and predict the supramolecular ordering behaviour of similar peptide sequences for biomaterial applications.

Methods

Phe-Wang resin, *O*-benzotriazole-*N*,*N*,*N*,*N*′-tetramethyl-uronium-hexafluoro-phosphate (HBTU), and Fmoc protected L-leucine were purchased from GL Biochem Ltd. Fmoc-protected D-leucine was purchased from Mimotopes. All solvents purchased were of analytical grade from Merck. Piperidine, trifluoroacetic acid (TFA), diisopropyl ethyl amine (DIPEA), triisopropyl silane (TIPS) were from Acros. Sodium dihydrogen phosphate and disodium hydrogen phosphate were from BDH AnalaR. High purity Milli-Q-water (MQ water) with a resistivity greater than 18 MΩ cm was obtained from an in-line Millipore RiOs/Origin system. Silicon wafers (M.M.R.C Pty Ltd.) were cleaned by ultrasonication (1 h) in a surfactant solution of 2% ethanol with 2% RBS 35 (Pierce) followed by rinsing with copious amounts of MQ water and dried with nitrogen, then cleaned for 1 h in a UV/ozone Procleaner™ (Bioforce Nanosciences). ^{1}H-NMR spectra were recorded at 400 MHz, and ^{13}C-NMR spectra were recorded at 100 MHz on a Bruker Instrument Biospin Av400H. Chemical shifts are reported in ppm relative to TMS. Low resolution ESI-MS spectra were acquired with a Shimadzu LCMS-2010EV mass spectrometer using a cone voltage of 50 V and the source was maintained at 80 °C. The solvent used was methanol containing 0.1% formic acid with a flow rate of 0.1 ml min^{-1}.

Peptide synthesis and purification

Both peptides were synthesised using standard Fmoc solid phase peptide synthesis with HBTU activation, following the same procedure described previously.[26] Crude peptides were too hydrophobic to be precipitated in cold ether, thus the majority of TFA was evaporated under nitrogen flow, and the remaining oil was redissolved in a mixture of acetonitrile–water, and then freeze-dried overnight. The freeze-dried product was purified by reverse-phase HPLC (Agilent Technologies). The HPLC was equipped with a preparative gradient pump (1100/1200), a preparative C-18 column (Luna, 10 microns, 100 Å, 150 × 21.20 mm, Phenomenex), an autosampler (G2260), and a diode array detector (G1365D). The gradient used consisted of acetonitrile (AcN)–water with 0.1% TFA with the following program: t = 0–3 min, 25% AcN; t = 15 min, 55% AcN; t = 16–20 min, 95% AcN. Compounds were freeze-dried and their purity verified by HPLC with the same equipment described above, but on an analytical C-18 column (Luna, 5 microns, 100 Å, 150 × 4.60 mm, Phenomenex; gradient 5–95% AcN over 15 minutes; t_R = 8 min for LFF; t_R = 9 min for ^{D}LFF, as shown in the ESI†). Peptide identity was verified by ESI-MS, ^{1}H-NMR and ^{13}C-NMR.

Samples preparation

Typically, 4.0 mg of peptide were dissolved in 300 μl of 0.1 M sodium phosphate buffer, pH 11.8 (buffer A), with the aid of sonication for 5 min, then diluted 1 : 1 with another 300 μl of 0.1 M sodium phosphate buffer, pH 5.6–5.7 (buffer B) to yield a final pH of 7.4. Samples were sonicated for another 5 min, unless otherwise indicated in the text. All buffer solutions were filtered (0.2 μm) prior to use.

Circular dichroism (CD) spectroscopy

The secondary structure of the peptides was analysed using a 0.1 cm quartz cell on a Jasco J815 Spectropolarimeter, with 1s integrations, 1 accumulation and a step size of 1 nm with a band width of 1 nm over a range of wavelengths from 200 to 280 nm. Peptide samples freshly prepared in buffer A were diluted with buffer B directly in the CD cell, and the spectra were recorded after 15 min. Measurements were repeated at least 5 times, and to reduce the noise near 200 nm, their average was plotted.

Fourier Transform Infrared (FT-IR) spectroscopy

FT-IR spectra were collected on a Nicolet 6700 FT-IR spectrometer in ATR mode. Freshly prepared sonicated peptide samples were analysed. Alternatively, they were left to settle and gel for 24 h in a glass vial. As no significant difference was seen in the signal identity between the two time points, spectra at 24 h are reported. A portion of the gel was then transferred on a clean piece of silicon wafer (1 cm × 1 cm), then gently spread by pressing a coverslip on top, and dried under vacuum for 24 h. Dried samples on the silicon wafers were placed directly to the ATR crystal, facing down. Scans were between 1800 and 1500 cm^{-1} with 80 accumulations at a resolution of 4 cm^{-1}.

Rheometry

Dynamic time sweep rheological analysis was conducted on an Ares rheometer (TA Instruments, USA) with a 25 mm aluminium parallel plate geometry. A Peltier temperature controller was connected to the rheometer to maintain a temperature of 25 °C. Freshly prepared and sonicated peptide sample solutions were either immediately analysed, or left to settle for 24 h. A gap of 300 μm was set. Strain sweeps were

recorded using a frequency of 10 rad s^{-1}. Frequency sweeps were recorded using a controlled strain of 0.3%.

Thioflavin T confocal fluorescence microscopy

Gel precursor solutions were prepared as indicated above and 25 μl were immediately placed on wells of a "μ-Slide Angiogenesis" uncoated (Ibidi, Germany, through DKSH Australia). 25 μl of a solution of Thioflavin T (200 μM in 50 mM glycine–NaOH pH 7.5, 0.2 μm filtered) were placed on top. After 15 minutes, the slides were imaged on a Leica SP5 microscope (63× water immersion objective, NA 1.2, excitation 458 nm, emission 468–600 nm). Alternatively, gels prepared in glass vials as described above were left to settle, and at later time points (24 h, or up to 7 days) were transferred onto the slides, stained and imaged as described above. Samples treated and stained with an identical protocol but without the peptide, were used as control and did not reveal any of the fluorescent structures described in the text (data not shown).

Atomic Force Microscopy (AFM)

An Asylum Research MFP-3D atomic force microscope (Santa Barbara, CA, USA) was used to measure surface topography in tapping mode with ultrasharp silicon nitride tips (NSC15 non-contact silicon cantilevers, MikroMasch, Spain). The tips used in this study had a typical force constant of 40 N m^{-1} and a resonant frequency of 320 kHz. Typical scan settings involved the use of an applied piezo deflection voltage of 0.6–0.7 V at a scan rate of 0.7 Hz. All images were processed (1^{st} order flattening algorithm) and linescans were generated using Igor Pro software. Freshly prepared and sonicated peptide samples were spread onto a clean square of silicon wafer (1 cm × 1 cm) by gently pressing a glass coverslip on top. Samples were then dried in a vacuum oven at room temperature for 24 h. Alternatively, freshly prepared peptide samples were left to settle and gel for 24 h, or up to 3 days, after which a small part of the gel was transferred onto a clean square piece of silicon wafer and dried as described above.

Cryo-Transmission Electron Microscopy (cryo-TEM)

A laboratory-built humidity-controlled vitrification system was used to prepare the hydrogels for imaging in a thin layer of vitrified ice using cryo-TEM. Humidity was kept close to 80% for all experiments, and the ambient temperature was 22 °C. 200-mesh copper grids coated with a perforated carbon film (Lacey carbon film: ProSciTech, Qld, Australia) were used for all experiments. Grids were glow discharged in nitrogen for 5 seconds immediately before use. Hydrogels were prepared as described above with or without sonication, showing no significant difference in their structure. They were either analysed immediately after preparation, or at different time points (after 24 h, or up to 3 days). At the time of analysis, the hydrogels were disrupted by tapping against the glass vial, and samples were agitated with the pipette tip in order to liquefy them if possible. Approximately 4 μl aliquots of sample were pipetted onto each grid prior to plunging. In the case of samples which could not be liquefied adequately, the gel was smeared gently onto the grid. After 30 seconds adsorption time the grid was blotted manually using Whatman 541 filter paper, for approximately 6–10 seconds. Blotting time was optimised for each sample. The grid was then plunged into liquid ethane cooled by liquid nitrogen. Frozen grids were stored in liquid nitrogen until required. The samples were examined using a Gatan 626 cryoholder (Gatan, Pleasanton, CA, USA) and a Tecnai 12 Transmission Electron Microscope (FEI, Eindhoven, The Netherlands) at an operating voltage of 120 kV. At all times low dose procedures were followed, using an electron dose of 8–10 electrons per $Å^2$ for all imaging. Images were recorded using a Megaview III CCD camera and AnalySIS camera control software (Olympus) using magnifications in the range 40 000× to 110 000×.

TEM with negative staining

Carbon-coated 300-mesh copper grids were glow-discharged in nitrogen to render the carbon film hydrophilic. A 4 μl aliquot of the sample was pipetted onto each grid. After 30 seconds adsorption time the excess was drawn off using Whatman 541 filter paper, followed by staining with 2% aqueous potassium phosphotungstate at pH 7.2, for 10 seconds. Grids were air-dried until needed. Samples were examined using a Tecnai 12 Transmission Electron Microscope (FEI, Eindhoven, The Netherlands) at an operating voltage of 120 kV. Images were recorded using a Megaview III CCD camera and AnalySIS camera control software (Olympus). Each grid was systematically examined and imaged to reflect a representative view of the sample. This was important as samples of this type can be very non-homogeneous on the grid; they tend not to disperse evenly and the structures occur in distinct patches.

X-Ray fiber Diffraction (XRD)

A Bruker D8 Advance X-ray Diffractometer with CuKα radiation (40 kV, 40 mA) equipped with a LynxEye silicon strip detector was employed to determine the X-ray diffraction (XRD) patterns. Each sample was scanned over the 2-theta range from 1° to 60° with a step size of 0.02° and a count time of 1.6 seconds per step. An air scatter slit was used to reduce the beam intensity at low angles. Analyses were performed on the collected XRD data for each sample using the Bruker XRD search match program EVA™. The samples were mounted on zero background plates consisting of a silicon wafer located in a standard Bruker specimen holder, and were dried in air prior to analysis.

Molecular modelling

Tripeptide structures were constructed in SybylX1.1 and model structures minimised using the AMBER force field, Kollman all atom charges, and implicit water (dielectric constant of 80). The minimisations were carried out by aligning copies of the tripeptides in an anti-parallel alignment with the distances between backbone amides being set to the optimum hydrogen bonding distance (2.7 Å). Steric clashes between the terminal Phe and Leu moieties were relieved by rotating the Phe rings away from the Leu (L-isomer) or leaving them in an extended conformation (D-isomer) with the backbones being set to a beta-sheet conformation. The centre Phe rings were aligned parallel to each other to maximise any π–π stacking interactions. The structures generated this way were then subjected to energy minimisation also

using the same force field charge model and solvent conditions as the single peptide chains described above.

Abbreviations

^{D}L	D-Leucine;
^{D}F	D-Phenylalanine;
^{D}V	D-Valine;
L	L-Leucine;
F	L-Phenylalanine;
V	L-Valine;
Fmoc	Fluorenylmethyloxy-carbonyl;
FT-IR	Fourier-Transformed Infrared;
XRD	X-Ray Diffraction.

Acknowledgements

The authors acknowledge: Firdawosia Kushkaki for the synthesis of the two peptides; the facilities of Monash Micro Imaging, Monash University, Australia, and in particular Stephen Firth, Dr Judy Callaghan and Dr Alex Fulcher for their scientific and technical assistance. The authors also acknowledge the CSIRO – Monash University Collaborative Research Support Scheme (CRSS) for funding.

Notes and references

1 A. L. Boyle and D. N. Woolfson, *Chem. Soc. Rev.*, 2011, **40**, 4295–4306.
2 L. E. R. O'Leary, J. A. Fallas, E. L. Bakota, M. K. Kang and J. D. Hartgerink, *Nat. Chem.*, 2011, **3**, 821–828.
3 X.-D. Xu, L. Liang, C.-S. Chen, B. Lu, N.-L. Wang, F.-G. Jiang, X.-Z. Zhang and R.-X. Zhuo, *ACS Appl. Mater. Interfaces*, 2010, **2**, 2663–2671.
4 A. Altunbas, N. Sharma, M. S. Lamm, C. Yan, R. P. Nagarkar, J. P. Schneider and D. J. Pochan, *ACS Nano*, 2009, **4**, 181–188.
5 D. J. Adams, *Macromol. Biosci.*, 2011, **11**, 160–173.
6 J. J. Panda, R. Dua, A. Mishra, B. Mittra and V. S. Chauhan, *ACS Appl. Mater. Interfaces*, 2010, **2**, 2839–2848.
7 Z. Yang, G. Liang, M. Ma, Y. Gao and B. Xu, *Small*, 2007, **3**, 558–562.
8 P. Ung and D. A. Winkler, *J. Med. Chem.*, 2011, **54**, 1111–1125.
9 M. Ma, Y. Kuang, Y. Gao, Y. Zhang, P. Gao and B. Xu, *J. Am. Chem. Soc.*, 2010, **132**, 2719–2728.
10 E. K. Johnson, D. J. Adams and P. J. Cameron, *J. Am. Chem. Soc.*, 2010, **132**, 5130–5136.
11 V. Jayawarna, M. Ali, T. A. Jowitt, A. E. Miller, A. Saiani, J. E. Gough and R. V. Ulijn, *Adv. Mater.*, 2006, **18**, 611–614.
12 A. Mishra, Y. H. Loo, R. S. Deng, Y. J. Chuah, H. T. Hee, J. Y. Ying and C. A. E. Hauser, *Nano Today*, 2011, **6**, 438.
13 C. A. E. Hauser, R. Deng, A. Mishra, Y. Loo, U. Khoe, F. Zhuang, D. W. Cheong, A. Accardo, M. B. Sullivan, C. Riekel, J. Y. Ying and U. A. Hauser, *Proc. Natl. Acad. Sci. U. S. A.*, 2011, **108**, 1361–1366.
14 R. Orbach, L. Adler-Abramovich, S. Zigerson, I. Mironi-Harpaz, D. Seliktar and E. Gazit, *Biomacromolecules*, 2009, **10**, 2646–2651.
15 H. M. Wang, C. H. Yang, M. Tan, L. Wang, D. L. Kong and Z. M. Yang, *Soft Matter*, 2011, **7**, 3897–3905.
16 A. Mahler, M. Reches, M. Rechter, S. Cohen and E. Gazit, *Adv. Mater.*, 2006, **18**, 1365–1370.
17 L. Adler-Abramovich, L. Vaks, O. Carny, D. Trudler, A. Magno, A. Caflisch, D. Frenkel and E. Gazit, *Nat. Chem. Biol.*, 2012, **8**, 701–706.
18 I. W. Hamley, *Angew. Chem., Int. Ed.*, 2007, **46**, 8128–8147.
19 A. M. Smith, R. J. Williams, C. Tang, P. Coppo, R. F. Collins, M. L. Turner, A. Saiani and R. V. Ulijn, *Adv. Mater.*, 2008, **20**, 37–41.
20 C. J. Bowerman, W. Liyanage, A. J. Federation and B. L. Nilsson, *Biomacromolecules*, 2011, **12**, 2735–2745.
21 M. Hughes, P. W. Frederix, J. Raeburn, L. S. Birchall, J. Sadownik, F. C. Coomer, I. H. Lin, E. J. Cussen, N. T. Hunt, T. Tuttle, S. J. Webb and D. J. Adams, *Soft Matter*, 2012, **8**, 5595–5602.
22 M. Reches and E. Gazit, *Science*, 2003, **300**, 625–627.
23 L. Adler-Abramovich, N. Kol, I. Yanai, D. Barlam, R. Z. Shneck, E. Gazit and I. Rousso, *Angew. Chem., Int. Ed.*, 2010, **49**, 9939–9942.
24 P. Tamamis, L. Adler-Abramovich, M. Reches, K. Marshall, P. Sikorski, L. Serpell, E. Gazit and G. Archontis, *Biophys. J.*, 2009, **96**, 5020–5029.
25 C. H. Gorbitz, *Chem. Commun.*, 2006, 2332–2334.
26 S. Marchesan, C. D. Easton, F. Kushkaki, L. Waddington and P. G. Hartley, *Chem. Commun.*, 2012, **48**, 2195–2197.
27 S. Y. Venyaminov and N. N. Kalnin, *Biopolymers*, 1990, **30**, 1259–1271.
28 N. S. de Groot, T. Parella, F. X. Aviles, J. Vendrell and S. Ventura, *Biophys. J.*, 2007, **92**, 1732–1741.
29 J. E. Shea, C. Wu, M. Biancalana and S. Koide, *J. Mol. Biol.*, 2009, **394**, 627–633.
30 Y. Goto, H. Yagi, T. Ban, K. Morigaki and H. Naiki, *Biochemistry*, 2007, **46**, 15009–15017.
31 I. W. Hamley, J. Adamcik, V. Castelletto, S. Bolisetty and R. Mezzenga, *Angew. Chem., Int. Ed.*, 2011, **50**, 5495–5498.
32 L. C. Serpell, *Biochim. Biophys. Acta, Mol. Basis Dis.*, 2000, **1502**, 16–30.
33 J. Liu, Q. Zheng, Y. Deng, N. R. Kallenbach and M. Lu, *J. Mol. Biol.*, 2006, **361**, 168–179.
34 D. Dhe-Sirano, E. D. Werner, N. Masahiro, L. Hansen, Y. I. Chi and S. E. Shoelson, *Nat. Struct. Mol. Biol.*, 2004, **11**, 968–974.
35 M. Nishi, E. D. Werner, B. C. Oh, J. D. Frantz, S. Dhe-Paganon, L. Hansen, J. Lee and S. E. Shoelson, *Mol. Cell. Biol.*, 2005, **25**, 2607–2621.
36 F. Porcelli, B. A. Buck-Koehntop, S. Thennarasu, A. Ramamoorthy and G. Veglia, *Biochemistry*, 2006, **45**, 5793–5799.
37 C. T. Webb, M. A. Gorman, M. Lazarou, M. T. Ryan and J. M. Gulbis, *Mol. Cell*, 2006, **21**, 123–133.
38 O. S. Makin, E. Atkins, P. Sikorski, J. Johansson and L. C. Serpell, *Proc. Natl. Acad. Sci. U. S. A.*, 2005, **102**, 315–320.
39 M. R. Sawaya, S. Sambashivan, R. Nelson, M. I. Ivanova, S. A. Sievers, M. I. Apostol, M. J. Thompson, M. Balbirnie, J. J. W. Wiltzius, H. T. McFarlane, A. O. Madsen, C. Riekel and D. Eisenberg, *Nature*, 2007, **447**, 453–457.
40 J. E. Shea and G. Bellesia, *J. Chem. Phys.*, 2009, **131**, 111102–111104.
41 C. Goldsbury, P. Frey, V. Olivieri, U. Aebi and S. A. Maller, *J. Mol. Biol.*, 2005, **352**, 282–298.

